Post-perovskite phase in selected sesquioxides from density-functional calculations

Razvan Caracas[1,2] and R. E. Cohen[1]
[1]*Geophysical Laboratory, Carnegie Institution of Washington, 5251 Broad Branch Road, North West, Washington DC 20015, USA*
[2]*Bayerisches Geoinstitut, University of Bayreuth, Universitaetstrasse 30, D-95446 Bayreuth, Germany*
(Received 22 July 2007; revised manuscript received 17 September 2007; published 1 November 2007)

We search for the existence of the post-perovskite structure in several nonmagnetic M_2O_3 sesquioxides using density-functional calculations. For each material we consider the corundum, Rh_2O_3-type II, perovskite, and post-perovskite structures. The perovskite structure is unstable with respect to at least one of the other structures at all pressures for all materials. The post-perovskite structure is stable above 120 GPa in Al_2O_3, above 344 GPa in Rh_2O_3, above 136 GPa in Ga_2O_3, and above 47 GPa in In_2O_3.

DOI: 10.1103/PhysRevB.76.184101 PACS number(s): 62.50.+p, 91.60.Gf, 78.30.−j, 81.30.Hd

I. INTRODUCTION

$MgSiO_3$ perovskite is the high-pressure silicate mineral that received much attention lately from both the solid-state theoreticians and experimentalists.[1–4] This mineral is the main component of the Earth's lower mantle. For decades it was believed that the perovskite structure is its final polymorph at high pressure before the decomposition into oxides. Recently it was shown that it undergoes a phase transition to an even more compact structure[1–3] at thermodynamic conditions (about 120 GPa and 2500 K) similar to the ones presumably found at the top of the D'' layer, the lowermost part of the Earth's mantle.[2,4] This transition to a post-perovskite phase answered questions related to the formation of the D'' layer and offered reasonable explanations to most seismic observations.[4–8]

The experimental difficulties related to obtaining the post-perovskite phase in $MgSiO_3$, due to the large transition pressures and temperatures and to the transparency of the pure material to laser, determined scientists to search for analogous materials, where a similar phase transition sequence is observed, but at lower pressures and/or temperatures. These analogous materials ideally present similar physical properties as the phase of interest, and are more easily observed. Traditionally germanates were considered good approximants for silicates and as the transition to post-perovskite in $MgGeO_3$ occurs about 30 GPa below that in $MgSiO_3$,[9] this compound was already used in mechanical or structural studies.[10,11] $NaMgF_3$ mimics the sequence of the phase transitions from perovskite to post-perovskite,[12] and possibly shows a transition to a post-post-perovskite phase.[13] $CaIrO_3$ has the post-perovskite structure at ambient conditions and is currently considered as its archetype.[14,15]

Based on the discovery of the post-perovskite phase in several sesquioxides (oxides with general formula M_2O_3, where M is a trivalent cation), such as Fe_2O_3 (Ref. 16 and 17) or Mn_2O_3 (Ref. 18) we initiated a series of theoretical investigations of the phase diagrams of sesquioxides. We select several nonmagnetic compounds Rh_2O_3, Al_2O_3, Ga_2O_3, and In_2O_3 whose phase diagrams have the highest chances of similarity with the silicates. We do not consider here transitional-metals magnetic oxides to avoid possible complications in the phase diagrams due to pressure-induced spin transitions.

For the selected materials we check the stability under pressure of the post-perovskite structure relative to the corundum, the Rh_2O_3-type-II, and the perovskite structures. Other potential structures, such as those developed by certain rare-earth sesquioxides, e.g., bixbyite or rhombohedral perovskite, were considered less compact than post-perovskite based on previous experience with Al_2O_3 (Ref. 19) and neglected.

II. COMPUTATIONAL DETAILS

We perform static first-principles calculations based on the local density approximation (LDA) of the density functional theory (DFT),[20,21] as implemented in the ABINIT package,[22,23] which is based on planewaves and pseudopotentials. We use Troullier-Martins pseudopotentials generated with the FHI98PP code.[24]

We employ a 38 Ha (1 Ha=27.2116 eV) kinetic energy cutoff for the plane waves and sample the reciprocal space using $4\times4\times4$ grids of special high-symmetry **k** points[25] for all structures. These parameters ensure an accuracy of the calculations on the order of the gigapascal in pressure and on the order of mili-Hartree in energy.

All the calculations are performed using the primitive lattices. We fully relax the structures (residual forces less than 5.0×10^{-5} Ha/Bohr and nonhydrostatic stresses of less than 10^{-2} GPa) under symmetry constraints for each chemical composition at several pressures. We compare the enthalpy differences to obtain the static transition pressures. We fit third order Birch-Murnagham equations of state on the static pressure-volume relations. The dynamical matrices, Born effective charges and dielectric permittivity tensors, were computed within density-functional perturbation theory, using the responses to atomic displacements and homogeneous electric fields.[26–29]

III. CRYSTAL STRUCTURES

Figure 1 shows the crystal structures of the four polymorphs we consider in this study: corundum, Rh_2O_3-type-II, perovskite, and post-perovskite.

Corundum structure is rhombohedral, with $R\bar{3}c$ space group and six formula units (Z) per unit cell in hexagonal setting. The cations lay in $12c(0\ 0\ z)$ Wyckhoff positions and

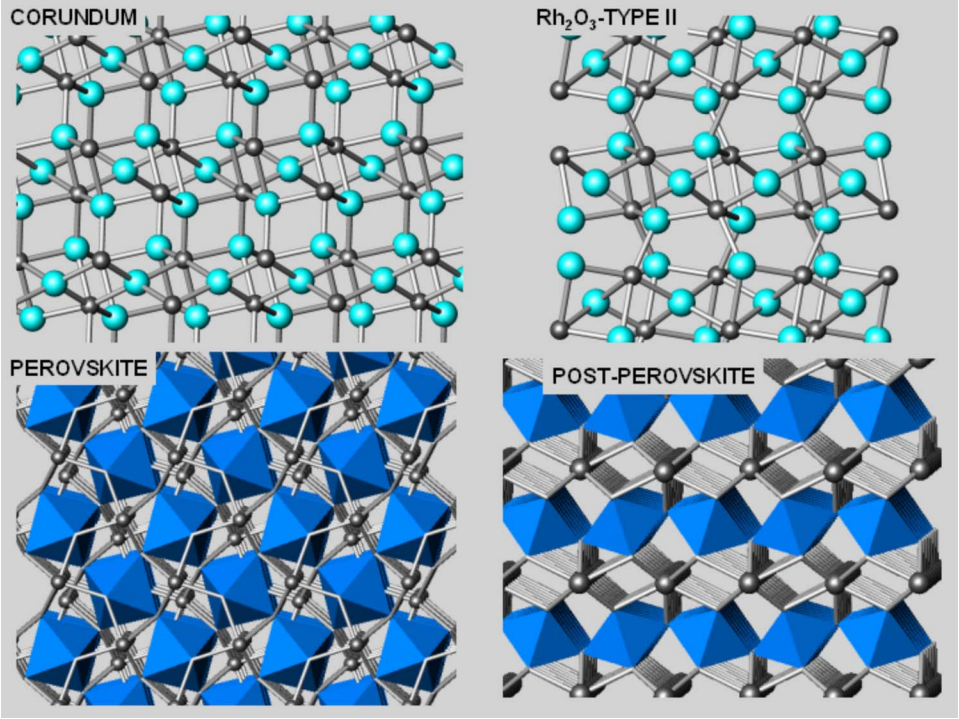

FIG. 1. (Color online) Crystal structure of the four polymorphs considered in this study. Smaller spheres are cations and larger spheres the anions. Corundum structure is rhombohedral and the three other structures are orthorhombic. For sake of clarity we explicitly show the MeO_6 octahedra for the perovskite and the post-perovskite structures.

the oxygen atoms in 18e(x 0 1/4) Wyckhoff positions.

Rh_2O_3-type-II structure is orthorhombic with *Pbcn* symmetry and Z=4, the cations in 8d(x y z) and the oxygen atoms in the 4c(0 y 1/4) and 8d(x y z) Wyckhoff positions. Rh_2O_3-type-II structure is a distortion of the corundum structure.

Perovskite has *Pbnm* space group and Z=4 with the cations in 4b(0 0 1/2) and 4c(x 1/4 z) and the oxygen atoms in 4c(x 1/4 z) and 8d(x y z) Wyckhoff positions. It is an orthorhombic distortion from the ideal cubic perovskite phase, with the octahedra tilted around two cartesian axes and the divalent cations displaced away from the center of the cubes.

TABLE I. The structural parameters of the post-perovskite phase of In_2O_3 computed at several pressures.

P (GPa)	a (Å)	b (Å)	c (Å)	
0	3.074	10.195	7.392	
10	3.033	10.055	7.242	
30	2.967	9.835	7.044	
60	2.896	9.583	6.850	
90	2.842	9.391	6.711	
120	2.799	9.221	6.610	
P	In_x	O_x	O_x	O_z
0	0.251	0.102	0.356	0.430
10	0.251	0.101	0.355	0.431
30	0.250	0.100	0.353	0.433
60	0.250	0.099	0.351	0.434
90	0.249	0.099	0.350	0.435
120	0.249	0.098	0.349	0.435

It corresponds to $a^-a^-c^+$ octahedral tilting,[30] which represents combinations of phonon instabilities in the M and R points of the ideal cubic reciprocal cell.[23] Perovskite is a three-dimensional framework structure build of octahedra that each share one oxygen anion with each of its six neighbors neighbors along each of the three cartesian directions of the space. The center of the octahedra are occupied by the cations in the 4b site and the interoctahedral spaces the octahedra are occupied by the cations in the 4c sites.

Post-perovskite has orthorhombic symmetry and *Cmcm* space group with Z=4. The cations lay in 4a(0 0 0) and 4c(0 y 1/4) and the oxygen atoms in 4c(0 y 1/4) and 8f(0 y z) Wyckhoff positions. The structure has a pronounced two-dimensional character and is formed of octahedral layers stacked in an $\cdots ABAB \cdots$ sequence. Within the layers the octahedra share one corner along one direction and one edge along the second direction; in the chosen setting

TABLE II. The dielectric tensors for the post-perovskite phase of In_2O_3 computed at several pressures.

P (GPa)	ϵ^∞
0	[6.84 6.02 6.47]
30	[5.85 5.17 5.28]
60	[5.41 4.88 4.85]
90	[5.17 4.72 4.64]
P (GPa)	ϵ^0
0	[18.06 15.78 85.47]
30	[13.52 12.06 31.19]
60	[12.20 10.51 25.29]
90	[11.77 9.62 24.79]

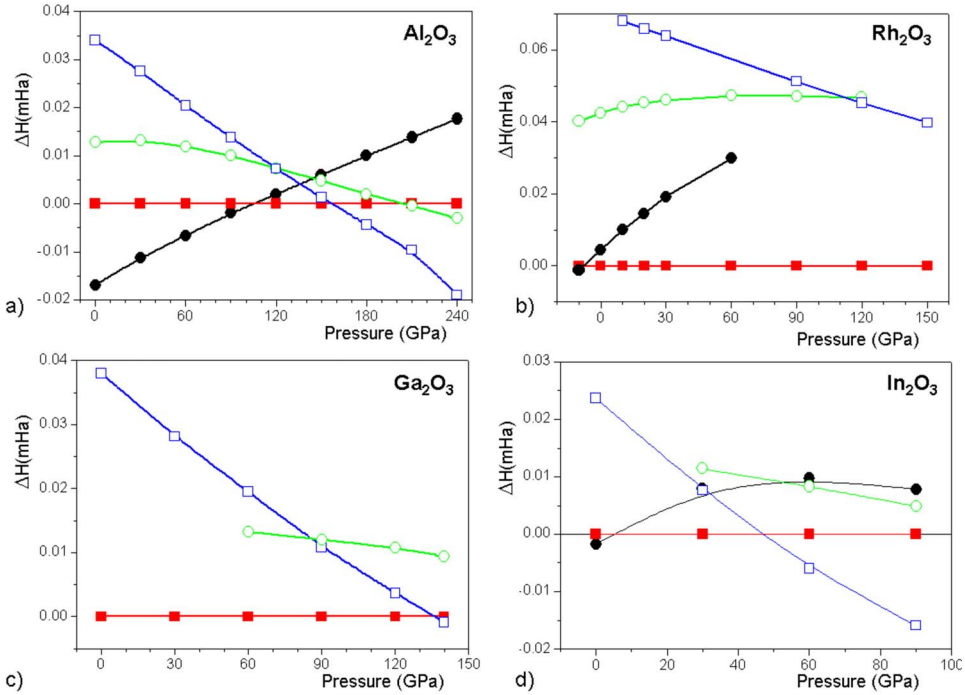

FIG. 2. (Color online) Enthalpies relative to the Rh_2O_3-type-II structure for Al_2O_3 (a), Rh_2O_3 (b), Ga_2O_3 (c), and In_2O_3 (d). For Rh_2O_3 the underestimation of the corundum to type-II transition pressure might be due to LDA. The transition to post-perovskite occurs at pressures around 360 GPa. For Ga_2O_3 the post-perovskite structure is stable above 136 GPa. For In_2O_3, the transition to post-perovskite occurs at about 47 GPa, making In_2O_3 a good candidate for the study of post-perovskite structure in sesquioxides and for the search of a possible post-post-perovskite phase. Corundum, type-II, perovskite, and post-perovskite structures are represented by, respectively, solid circles, solid squares, open circles, and open squares. Lines are guide for the eyes.

they correspond respectively to the [001] and [100] directions, with [010] perpendicular to the octahedral layer.

IV. PHASE DIAGRAMS

A. Al_2O_3

From all the sesquioxides alumina received the largest attention from the high-pressure community, due to its technological applications[31] and to its implications to the Earth's mineralogy.[32] The phase diagram was determined by several groups.[33–36] The sequence of phase transitions at low temperature is corundum—Rh_2O_3-type-II structure—post-perovskite, with transition pressures at, respectively 104 and 156 GPa.[33] The perovskite structure was found to be unstable with respect to at least one of the three other phases at all pressures [Fig. 2(a)]. A third order Birch-Murnagham equation of states fitted on the theoretical static pressure-volume results for the post-perovskite structure of Al_2O_3 give $V_0=25.91$ Å^3, $K_0=229$ GPa, and $K'=4.16$.

B. Rh_2O_3

The phase diagram of Rh_2O_3 is characterized by two structures at low pressures and temperatures, corundum and Rh_2O_3-type II with a room temperature transition pressure of 6.5 GPa.[37] At high temperatures the stable structure is Rh_2O_3-type III with *Pbca* space group.[38–40]

The static calculations rule out perovskite as a stable high-pressure phase [Fig. 2(b)]. According to our results the Rh_2O_3-type-II structure transforms to post-perovskite at about 360 GPa (obtained from the extrapolation of the enthalpy differences computed up to 150 GPa).

As the corundum to Rh_2O_3-type-II theoretical transition occurs 14 GPa below the experimental transition pressure (7 GPa at room temperature), most probably due to LDA pressure underestimation, the value of the transition to post-perovskite would have the same underestimation. The transition pressure to post-perovskite, even corrected down to 344 GPa, remains today beyond reasonable experimental reach. The stability range of the type-II structure makes this material a bad candidate in the study of the post-perovskite structure. The post-perovskite phase of Rh_2O_3 has $V_0=53.33$ Å^3, the smallest bulk modulus of all the four sesquioxides $K_0=162$ GPa and $K'=7.03$.

C. Ga_2O_3

The phase diagram of Ga_2O_3 at low pressures is characterized by several ordered and disordered structures.[41] At higher pressures the corundum structure is stable, but apparently disordered.[42] We did not calculate the stability field of the corundum structure due to its disordered character and because we are more interested by the behavior at higher pressures and the possible appearance of the post-perovskite structure.

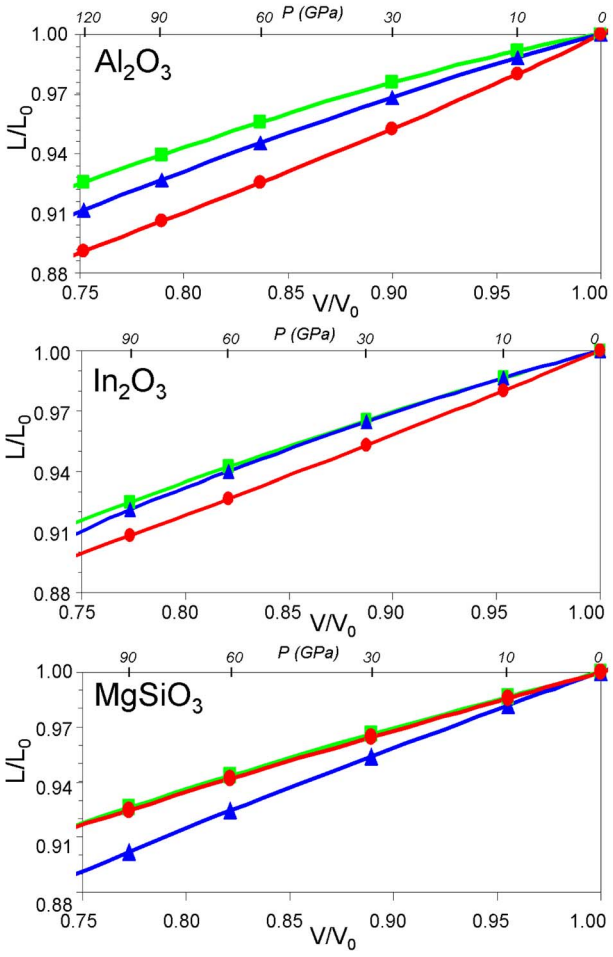

FIG. 3. (Color online) Compressibility of the lattice parameters of the post-perovskite structure, L/L_0 as a function of the bulk compressibility, V/V_0 in Al_2O_3, In_2O_3, and $MgSiO_3$. Squares, triangles, and circles denote the a, b, and c lattice parameters, respectively.

The static theoretical phase diagram that we obtain for Ga_2O_3 is presented in Fig. 2(b). The Rh_2O_3-type-II structure is stable up to about 136 GPa where post-perovskite becomes more stable. At the transition the volume drop is about 3.6%. The perovskite structure is unstable at all pressures with respect to the Rh_2O_3-type-II or the post-perovskite structures.

The parameters of the third-order Birch-Murnagham equation of state for post-perovskite are $V_0=44.99$ Å^3, $K_0=263$ GPa, and $K'=3.86$. From the sesquioxides studied here Ga_2O_3 has the largest bulk modulus.

D. In_2O_3

Most of the studies of In_2O_3 focused on thin films and doping to enhance its properties. In_2O_3 exhibits the corundum structure as a high-pressure polymorph.[43] To our best knowledge this study is the first high-pressure investigation of In_2O_3 above the corundum structure.

Figure 2(c) shows the relative enthalpy differences between the four considered structures for In_2O_3. Corundum is the stable structure at 0 GPa. With increasing pressure at about 5 GPa it transforms to the Rh_2O_3-type-II structure. The volume drop at the transition pressure is about 2.5%. The Rh_2O_3-type-II structure transforms to post-perovskite at 47 GPa. This low transition pressure to post-perovskite makes In_2O_3 the best analog for post-perovskite from all the sesquioxides studied so far and also a promising candidate in the search for a post-post-perovskite phase. The volume drop at the transition is about 3.1%. The structural parameters of the post-perovskite phase as computed in LDA at several pressures are given in Table I. The post-perovskite phase has $V_0=57.96$ Å^3, $K_0=187$ GPa, and $K'=4.77$. The perovskite structure is unstable to at least one of the other three structures at all pressures.

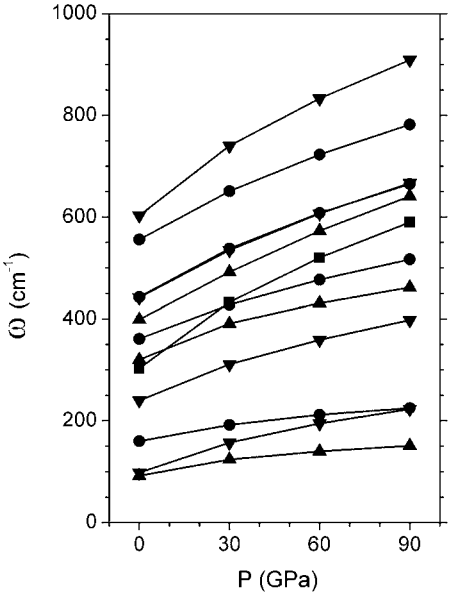

FIG. 4. Pressure variation of the g modes in the post-perovskite phase of In_2O_3. There are 12g modes that decompose as $4A_g+3B_{1g}+1B_{2g}+4B_{3g}$. Circles, down-pointing triangles, squares, and up-pointing triangles denote, respectively, A_g, B_{1g}, B_{2g}, and B_{3g} modes.

V. COMPARISON OF THE POST-PEROVSKITE STRUCTURE IN SESQUIOXIDES AND IN SILICATES

Despite sustained efforts we could not identify any apparent relation between the transition pressures and the geometrical characteristics of the cations, such as covalent or ionic radii. However, we may perform a comparison between the high-pressure behavior of the silicates and sesquioxides.

We calculate the compressibility of the three lattice parameters of the conventional cell of the post-perovskite structure, a/a_0, b/b_0, and c/c_0 as a function of bulk compression V/V_0 and exemplify in Fig. 3 with Al_2O_3, In_2O_3, and $MgSiO_3$. The b/a and the c/a ratios, as a measure of the structural anisotropy, do not present an obvious trend with chemistry. We observe that the compressibility of the sesquioxides is relatively different from the compressibility of the silicates. In sesquioxides the applied pressure reduces more

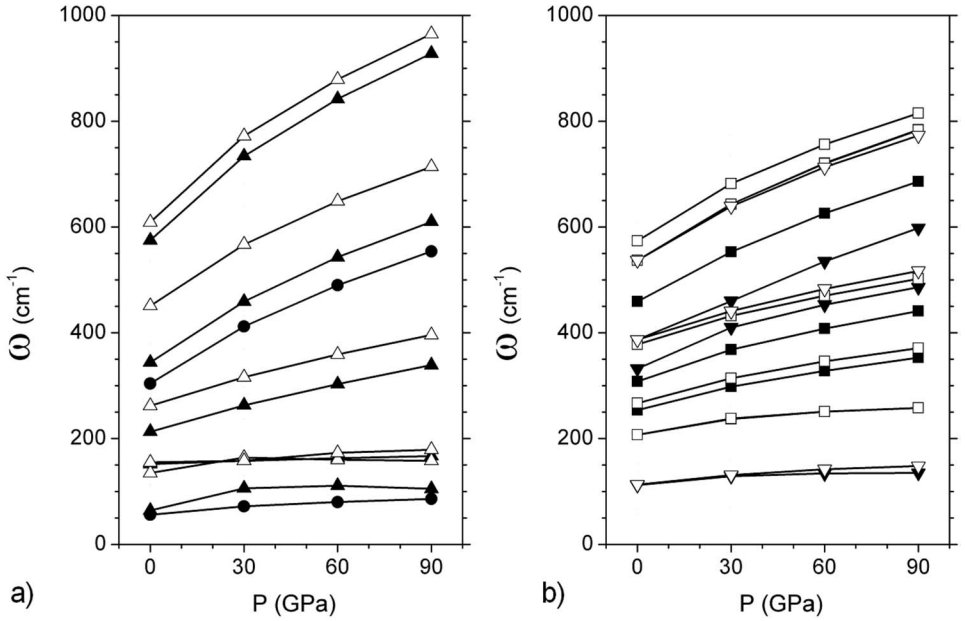

FIG. 5. Pressure variation of the u modes in the post-perovskite phase of In_2O_3. (a) A_u and B_{1u} modes and (b) B_{2u} and B_{3u} modes. There are 15 optical u modes that decompose as $2A_u+5B_{1u}+5B_{2u}+3B_{3u}$. Circles, down-pointing triangles, squares, and up-pointing triangles denote, respectively, A_u, B_{1u}, B_{2u}, and B_{3u} modes. Full symbols are for the TO modes and empty symbols for the LO modes.

in-plane the octahedral layers than it diminishes the interlayer space. The compressibility of the layers is more significant along the c axis (the direction of the corner sharing) than the a axis (the direction of the edge sharing). This larger compressibility is accommodated by rotations of the octahedra around the shared O atom. In silicates the pressure reduces preferentially the interlayer distance. The compressibility of the octahedral layers is also more isotropic in silicates than in sesquioxides.

Because in sesquioxides the same chemical bonds exist within both the octahedral layers and in the interlayer space the accommodation of compression involves a large amount of structural rearrangement. This is more than in silicates where the compression involves differential reduction of the various cation-anion bonds, some (Mg-O) more compressible than others (Si-O).

The Me-O-Me angles, where Me is the octahedrally coordinated cation, has larger values in the silicates, in the 134°–147° range, than in the sesquioxides, in the 102°–129° range. This different behavior in compressibilities suggests that sesquioxides should be employed with care as analogs to the silicates for the study of different physical properties.

VI. ZONE-CENTER LATTICE DYNAMICS OF THE POST-PEROVSKITE PHASE IN In_2O_3

Because In_2O_3 is the most promising of the studied sesquioxides to find the post-perovskite structure, we report in the following its full lattice dynamical properties as a function of pressure and the theoretical Raman spectra, information that can be useful also as an identification tool for the phase transition.

The values of the dielectric tensors ϵ^{∞} and ϵ^{0} computed at several pressures are listed in Table II. The values of the dielectric tensor decrease with increasing pressure. ϵ^{0} is highly anisotropic, much more than in $MgSiO_3$. The largest value is parallel to the [001] direction, along the corner-sharing direction of the octahedra.

The calculated Born effective charges $Z_{ij}^{\alpha *}=1/\Omega\ \delta P_i/\delta\tau_j^{\alpha}$, where Ω is the unit cell volume, P_i is the polarization along the direction i, and τ_j^{α} is the displacement of atom α along direction j at zero electric field, are listed in Table III. They are weakly anisotropic and their values are slightly anomalous with respect to the nominal charges, +3 for In and −2 for O, showing a mixed ionic and covalent In-O bonding. They show little variation with pressure, indicating a constancy of the character for the chemical bonds.

The 27 optical modes in the zone center of the post-perovskite structure (with space group $Cmcm$ and atoms in $4a$, $4c$, and $8f$ Wyckhoff positions) decompose as 12 g modes, $4\ A_g+3\ B_{1g}+1\ B_{2g}+4\ B_{3g}$, and 15 u modes, $2\ A_u+5\ B_{1u}+5\ B_{2u}+3\ B_{3u}$. Figures 4 and 5 show the pressure variation of the g modes and the u modes, respectively. With the exception of the lowest-in-frequency B_{3u} mode, all the other modes harden with pressure, at different rates. The structure does not show any mode softening in the zone-center over the 0–90 GPa pressure range.

Because of its utility as an identification tool of the transition to the post-perovskite structure,[44] we next compute the Raman spectra for powder crystalline In_2O_3 with post-perovskite structure. The Raman intensity for an oriented single-crystal depends on the frequency of the incident laser ω_L, on temperature T which are user-defined parameters, on the frequency of the Raman mode ω_i, and on the Raman tensor α_{xy}. We compute the Raman tensors using the ABINIT implementation of the density-functional perturbation theory.[45] We neglect the surface and the grain size effects and we perform integrals over all possible orientation of infinite ideal bulk crystals.[46–49]

The resulting computed Raman spectra are shown in Fig. 6. The Raman spectra show an interesting evolution with pressure. The intensity of the peaks decrease by about one fifth over the 0–90 GPa pressures range. The relative intensity of the different modes and thus the dominant modes also vary from one pressure to the other.

At low pressures the Raman spectrum is dominated by the A_g mode (443 cm^{-1} at 0 GPa), which is superposed on a B_{3g} mode (442 cm^{-1} at 0 GPa). The A_g mode is a breathing-like mode of the InO_6 octahedra, and B_{3g} is the Si-O-Si bending mode corresponding to the tilting of the octahedra around the shared oxygen atom, coupled with small displacements of the In atoms from the interlayer space. Under pressure their intensity is drastically reduced compared to the other modes. At 60 GPa (A_g 477 and B_{3g} at 359) together they represent about 11% of the intensity of the main peak.

The second most intense mode at 0 GPa, A_g at 361 cm^{-1}, is a Si-O-Si bending similar to B_{3g} described above. Its relative intensity increases and this mode becomes the dominant mode at higher pressures.

The B_{2g} mode (303 cm^{-1} at 0 GPa) consists of vibrations of the sublattice of oxygen atoms that belong to the edges shared by the octahedra from the octahedral layer. The oxygen atoms move in columns along the edge-sharing direction, alternately along the [010] direction, such as to shear the octahedra. Its relative intensity also diminishes with pressure.

The low-frequency B_{3g} mode (195 cm^{-1} at 0 GPa) involves the sublattice of In atoms from the interlayer space together with the oxygen atoms that are edge shared. Large fragments of the In coordination polyhedra from the interlayer space vibrate against each other along the [001] direction. The relative intensity of this mode increases with pressure and it becomes the second most important mode at 60 GPa.

The high-frequency A_g mode (556 cm^{-1} at 0 GPa and 723 cm^{-1} at 60 GPa) is a breathinglike mode of the polyhedra from the interlayer space. The measured Raman spectra of Mn_2O_3 with post-perovskite structure[50] are similar to the spectra of In_2O_3. The computed spectra of $MgSiO_3$ are similar to the ones of In_2O_3 only at low pressures; at high pressures the spectra of $MgSiO_3$ are largely dominated by only

TABLE III. Eigenvalues of the Born effective charges for the post-perovskite phase of In_2O_3 computed at several pressures. Because of symmetry the charges of In_1 and O_1 atoms are diagonal. The charges of the In_2 and O_2 have small non-zero off-diagonal values on the 23 position, not shown here.

P=0 GPa	
In_1	[3.900 3.394 3.802]
In_2	[3.095 3.593 3.603]
O_1	[−1.932 −2.357 −2.576]
O_2	[−1.846 −2.635 −2.780]
P=30 GPa	
In_1	[3.768 3.352 3.688]
In_2	[3.072 3.513 3.518]
O_1	[−1.933 −2.317 −2.451]
O_2	[−1.895 −2.534 −2.676]
P=60 GPa	
In_1	[3.693 3.313 3.618]
In_2	[3.063 3.468 3.489]
O_1	[−1.939 −2.290 −2.386]
O_2	[−1.911 −2.482 −2.621]
P=90 GPa	
In_1	[3.641 3.279 3.569]
In_2	[3.058 3.444 3.475]
O_1	[−1.946 −2.270 −2.344]
O_2	[−1.921 −2.447 −2.585]

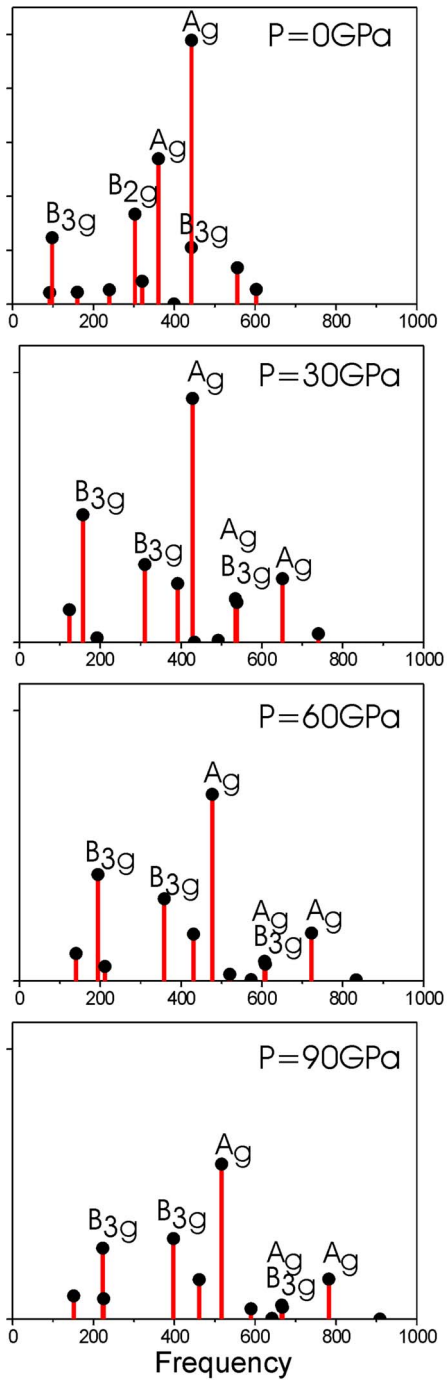

FIG. 6. (Color online) The calculated powder Raman spectra of crystalline In_2O_3 with post-perovskite structure at several pressures.

one mode, which will not be the case for In_2O_3.

VII. CONCLUSIONS

In a search for $MgSiO_3$ post-perovskite analogs we performed static (0 K) first-principles calculations to investigate the stability of several high-density structures in a series of nonmagnetic sesquioxides. We computed the relative stability of the corundum, Rh_2O_3-type-II, perovskite, and post-perovskite structures. We find that perovskite is unstable to at least one of the other three structures at all pressures. We predict that the post-perovskite structure is stable in Rh_2O_3 above 344 GPa, in Al_2O_3 above 120 GPa, in Ga_2O_3 above 136 GPa, and in In_2O_3 above 47 GPa. Based on similarities with Al_2O_3 and with the low-pressure phase diagram of Rh_2O_3 we find probable that the temperature would increase these transition pressures. We compare the structural behavior of post-perovskite for sesquioxides and for $MgSiO_3$ and find important differences in the compressibilities. For In_2O_3 with post-perovskite structure we compute the zone-center lattice-dynamical properties and analyze, in detail, the Raman spectrum and its variation with pressure. With a large number of possible chemical combinations sesquioxides remain a promising field of investigation, in the search for new structures and for analogs for silicates, where In_2O_3 is for the moment the preferred candidate.

ACKNOWLEDGMENTS

The calculations were partly performed in the Michigan Supercomputers Center under NPACI Grant No. EAR 050012.

[1] M. Murakami, K. Hirose, K. Kawamura, N. Sata, and Y. Ohishi, Science **304**, 855 (2004).
[2] T. Tsuchiya, J. Tsuchiya, K. Umemoto, and R. M. Wentzcovitch, Earth Planet. Sci. Lett. **224**, 241 (2004).
[3] A. Oganov and S. Ono, Nature (London) **430**, 445 (2004).
[4] R. Caracas and R. E. Cohen, Geophys. Res. Lett. **32**, L16310 (2005).
[5] T. Tsuchiya, J. Tsuchiya, K. Umemoto, and R. M. Wentzcovitch, Geophys. Res. Lett. **31**, L14603 (2004).
[6] J. Wookey, S. Stackhouse, J. M. Kendall, J. Brodholt, and D. G. Price, Nature (London) **438**, 1004 (2005).
[7] I. Sidorin, M. Gurnis, and D. V. Helmberger, Science **286**, 1326 (1999).
[8] I. Sidorin, M. Gurnis, and D. V. Helmberger, J. Geophys. Res. **104**, 15 005 (1999).
[9] A. Kubo, B. Kiefer, G. Shen., V. B. Prakapenka, R. J. Cava, and T. S. Duffy, Geophys. Res. Lett. **33**, L12S12 (2006).
[10] K. Hirose, K. Kawamura, Y. Ohishi, S. Tateno, and N. Sata, Am. Mineral. **90**, 262 (2005).
[11] S. Merkel, A. Kubo, L. Miyagi, S. Speziale, T. S. Duffy, H.-K. Mao, and H.-R. Wenk, Science **311**, 644 (2006).
[12] H.-Z. Liu, J. Chen, J. Hu, C. D. Martin, D. J. Weidner, D. Hausermann, and H.-K. Mao, Geophys. Res. Lett. **32**, L04304 (2005).
[13] C. D. Martin, W. A. Crichton, H. Liu, V. Prakapenka, J. Chen, and J. B. Parise, Geophys. Res. Lett. **33**, L11305 (2006).
[14] K. Hirose and Y. Fujita, Geophys. Res. Lett. **32**, L13313 (2005).
[15] N. Miyajima, K Ohgushi, M. Ichihara, and T. Yagi, Geophys. Res. Lett. **33**, L12302 (2006).
[16] S.-H. Shim and T. S. Duffy, Am. Mineral. **87**, 318 (2001).
[17] S. Ono and Y. Ohishi, J. Phys. Chem. Solids **66**, 1714 (2005).
[18] J. Santillan, S.-H. Shim, G. Shen, and V. B. Prakapenka, Geophys. Res. Lett. **33**, L15307 (2006).
[19] W. Duan, R. M. Wentzcovitch and K. T. Thomson, Phys. Rev. B **57**, 10 363 (1998).
[20] P. Hohenberg and W. Kohn, Phys. Rev. **136**, B864 (1964).
[21] W. Kohn and L. J. Sham, Phys. Rev. **140**, A1133 (1965).
[22] X. Gonze, J.-M. Beuken, R. Caracas, F. Detraux, M. Fuchs, G.-M. Rignanese, L. Sindic, M. Verstraete, G. Zerah, F. Jollet, M. Torrent, A. Roy, M. Mikami, Ph. Ghosez, J.-Y. Raty, and D. C. Allan, Comput. Mater. Sci. **25**, 478 (2002).
[23] X. Gonze, G.-M. Rignanese, M. Verstraete, J.-M. Beuken, Y. Pouillon, R. Caracas, F. Jollet, M. Torrent, G. Zerah, M. Mikami, P. Ghosez, M. Veithen, V. Olevano, L. Reining, R. Godby, G. Onida, D. Hamann, and D. C. Allan, Z. Kristallogr. **220**, 558 (2005).
[24] M. Fuchs, M. Scheffler, Comput. Phys. Commun. **119**, 67 (1999).
[25] H. J. Monkhorst and J. D. Pack, Phys. Rev. B **13**, 5188 (1976).
[26] X. Gonze, Phys. Rev. B **55**, 10337 (1997).
[27] X. Gonze and C. Lee, Phys. Rev. B **55**, 10355 (1997).
[28] S. Baroni, S. de Gironcoli, A. Dal Corso, and P. Giannozzi, Rev. Mod. Phys. **73**, 515 (2001).
[29] X. Gonze, G.-M. Rignanese, and R. Caracas, Z. Kristallogr. **220**, 458 (2005).
[30] A. M. Glazer, Acta Crystallogr., Sect. B: Struct. Crystallogr. Cryst. Chem. **28**, 3384 (1972).
[31] K. T. Thomson, R. M. Wentzcovitch, and M. S. T. Bukowinski, Science **274**, 1880 (1996).
[32] F. C. Marton and R. E. Cohen, Am. Mineral. **79**, 789 (1994).
[33] R. Caracas and R. E. Cohen, Geophys. Res. Lett. **32**, L06303 (2005).
[34] J. Tsuchiya, T. Tsuchiya, and R. M. Wentzcovitch, Phys. Rev. B **72**, 020103(R) (2005).
[35] S. Akber-Knutson, G. Steinle-Neumann, and P. D. Asimow, Geophys. Res. Lett. **32**, L14303 (2005).
[36] A. Oganov, and S. Ono, Proc. Natl. Acad. Sci. U.S.A. **102**, 10828 (2005).
[37] R. D. Shannon and C. T. Prewitt, J. Solid State Chem. **2**, 134 (1970).
[38] J. W. M. Biesterbos and J. Hornstra, J. Less-Common Met. **30**, 121 (1973).
[39] K. R. Poeppelmeier, J. M. Newsam, and J. M. Brown, J. Solid State Chem. **60**, 68 (1985).
[40] S. Zhuo and K. Sohlberg, J. Solid State Chem. **179**, 2126 (2006).
[41] R. Roy, V. G. Hill, and E. F. Osborn, J. Am. Chem. Soc. **74**, 719 (1952).
[42] D. Machon, P. F. McMillan, B. Xu, and J. Dong, Phys. Rev. B **73**, 094125 (2006).
[43] M. Epifani, P. Siciliano, A. Gurlo, N. Barsan, and U. Weimar, J.

Am. Chem. Soc. **126**, 4078 (2004).
[44] R. Caracas and R. E. Cohen, Geophys. Res. Lett. **33**, L12S05 (2006).
[45] M. Veithen, X. Gonze, and P. Ghosez, Phys. Rev. B **71**, 125107 (2005).
[46] S. A. Prosandeev, U. Waghmare, I. Levin, and J. Maslar, Phys. Rev. B **71**, 214307 (2005).
[47] G. Placzek, in *Handbuch der Radiologie* (Akademische Verlagsgeselschaft, Leipzig, 1934), Vol. 6, p. 208.
[48] W. Hayes and R. Loudon, *Scattering of Light by Crystals* (Wiley, New York, 1978), p. 113.
[49] H. Hamaguchi, Adv. Infrared Raman Spectrosc. **12**, 273 (1985).
[50] S. H. Shim, A. Kubo, and T. S. Duffy, Earth Planet. Sci. Lett. **260**, 166–178 (2007).